J Mater Sci: Mater Med (2009) 20:1427–1436
DOI 10.1007/s10856-009-3712-6

Chitosan reinforced apatite–wollastonite coating by electrophoretic deposition on titanium implants

Smriti Sharma · Vivek P. Soni · Jayesh R. Bellare

Received: 1 December 2008 / Accepted: 6 February 2009 / Published online: 1 March 2009

Abstract A novel bioactive porous apatite–wollastonite/chitosan composite coating was prepared by electrophoretic deposition. The influence of synthesis parameters like pH of suspension and current density was studied and optimized. X-ray diffraction confirmed crystalline phase of apatite–wollastonite in powder as well as composite coating with coat crystallinity of 65%. Scanning electron microscope showed that the porosity had interconnections with good homogeneity between the phases. The addition of chitosan increased the adhesive strength of the composite coating. Young's modulus of the coating was found to be 9.23 GPa. One of our key findings was sheet-like apatite growth unlike ball-like growth found in bioceramics. Role of chitosan was studied in apatite growth mechanism in simulated body fluid. In presence of chitosan, dense negatively charged surface with homogenous nucleation was the primary factor for sheet-like evolution of apatite layer. The results suggest that incorporation of chitosan with apatite–wollastonite in composite coating could provide excellent in vitro bioactivity with enhanced mechanical properties.

1 Introduction

Titanium and titanium alloys have shown high potential for load bearing in bioimplant applications due to their biocompatibility and reliable mechanical properties. But from a biochemical point of view, they are considered nearly inert materials [1–3]. It was discovered by Hench et al. in 1970 that various kind of glasses, glass ceramics and sintered ceramics bond to living bone. Glass–ceramics containing apatite and wollastonite crystals (AW) have been found to have high bioactivity and fairly high mechanical strength [4, 5]. Therefore, metallic implants coated with bioactive materials are able to induce a biological bonding with both soft and hard tissues.

Plasma sprayed hydroxyapatite, the most common commercially available coating, does have some drawbacks like compositional modifications and poor performance due to high temperature [6]. The inadequate adhesion of plasma spray coatings has led to investigation of other coating techniques. Electrophoretic deposition is known to be one of the most effective techniques to assemble fine particles because of its simplicity, low equipment cost, the possibility of deposition on substrates of complex shape, high purity and microsturctural homogeneity of deposits. Another important advantage of EPD is the possibility of room temperature processing and its suitability for co-deposition of various materials.

Although ceramic coatings were shown to have improved bone attachment and aided integration of implants, long term stability of coating is still a challenging issue. In order to improve the biocompatibility and mechanical strength of implant materials, attention has been directed towards the potential use of ceramic–polymer composites in recent days. The analysis of available literature indicates that chitosan can be promising biopolymer for fabrication of composite coating using EPD [7, 8]. Interest in chitosan for fabrication of composite coating stems from its excellent film forming property. Chitosan is a biopolymer (polymer of 2-amino 2-D-glucose) derived by

S. Sharma · V. P. Soni · J. R. Bellare (✉)
School of Biosciences and Bioengineering, Indian Institute of Technology Bombay, Powai, Mumbai 400076, India
e-mail: jb@iitb.ac.in

J. R. Bellare
Department of Chemical Engineering, Indian Institute of Technology Bombay, Powai, Mumbai, India

deacetylation of chitin, the principal constituent in shells of crabs, lobsters and other crustaceans. It has been used in number of biomedical applications such as drug encapsulation, fat absorption, and in wound dressing materials. It is non-toxic and biocompatible. Chitosan addition to keratin film showed increased flexural strength and also enhanced antibacterial properties [9]. Incorporation of chitosan to calcium phosphate coating has proven to be a more favorable surface for goat bone marrow stromal cell attachment [10]. Chitosan/wollastonite composite scaffolds have also been used for tissue engineering earlier [11].

A detailed insight into the mechanism of apatite formation on bioactive ceramics is considered to be of importance. The essential condition for a bone implant to bond to a living bone is the formation of a bone-like apatite layer on its surface. Bioactivity studies using SBF on wollastonite suggest that apatite growth is induced by formation of functional groups like Si–OH on their surfaces in body environment [12]. But this mechanism has not been studied thoroughly in presence of chitosan. In this study we investigated the changes in morphology of apatite growth in presence of biopolymer. Role of chitosan has been discussed with respect to surface charge distribution and a mechanism has been proposed.

In this work we have developed composite coating by EPD, and characterized it using various techniques. Various coating parameters were studied and optimized to get uniform and crack-free coat. Synergistic effect of chitosan with ceramic coating was studied in terms of reinforcement effect of biopolymer and bioactivity of composite coating.

2 Materials and methods

2.1 Preparation of materials used in electrophoretic deposition

Apatite–wollastonite (AW) powder formed by modified sol–gel route [13] was used in this study for synthesizing the composite coating. Briefly, an ionic solution of calcium nitrate and magnesium nitrate was prepared and mixed with organic solution of Tetraethyl Orthosilicate (TEOS), methanol and calcium fluoride in sol–gel apparatus. All analytical-grade chemicals were used. After the formation of gel, it was calcined at 200°C and then sintered at 950°C in tubular furnace (hcs-Tub, hecons, Mumbai). The powder obtained was ball milled at 150 rpm for 2 h. Particle sizing was carried out using a dynamic light scattering (BI-9000 AT Digital Autocorrelator, Brookhaven Instrument, USA) and was found to be 200 nm. Chitosan was obtained from Otto chemicals (98% Deacetylated). Titanium sheet (Manhar metal suppliers, Mumbai, India) of dimension (10 mm × 15 mm × 0.5 mm) was used as the test substrate. The substrates were etched with 2% hydrofluoric acid (HF) for 1 min, then rinsed with MilliQ water (Millipore) and air-dried before use.

2.2 Deposition details

Titanium (Ti) test samples were used as both anode and cathode. Distance between the electrodes was maintained at 10 mm. The ceramic particles of apatite–wollastonite were dispersed ultrasonically in ethanol for 30 min at 20 Hz (98 kW) in an ultrasonic vibrator. Electrophoretic deposition was performed from suspension of 2 g/l AW particles in ethanol. The pH of the ceramic suspension was optimized after carrying out repeated experiments and was fixed at pH of 1.6. Suspension of 0.2% of chitosan was prepared in 2% acetic acid solution. Cathodic deposition were performed on Ti sheet with coating area 10 mm × 10 mm. Current density was fixed to 3 mA/cm^2 to coat ceramic and 1 mA/cm^2 for chitosan. Repeated deposition method was applied to reduce formation of cracks in the coating. To start with, surface of titanium was coated with thin layer of chitosan followed by three alternate coating cycles of ceramic and chitosan to obtain homogenous composite coating. The last coat of chitosan was repeated two times so as to encapsulate composite coating by polymer thereby preventing the erosion of the final composite coating.

2.3 Characterization of composite coatings

Compositional phase analyses and crystallinity were determined using X-ray diffraction (XRD: X'Pert PANalytical, Philips). The operating conditions were 40 kV and 30 mA by using Cu Kα monochromatic radiation with a step size of 0.2°/15 s. Scanning electron microscopy (JSM-6400, JEOL, Japan) and EDAX was employed to investigate the morphological features and elemental composition. The working distance and voltage used during the scanning electron microscopy was 15 mm and 20 kV respectively. Micro-Raman investigations were performed on the localized area of the coated sample using Raman spectrometer (LabRAM HR800, Jobin Yvon, France). Ar^+ 514-nm laser source of intensity $\simeq$10 mW was used.

2.4 Mechanical testing of composite coatings

2.4.1 Tape test

For assessing the adhesion of the composite coating on titanium substrate, a standard test method (Tape test-ASTM D 3359-97) was used. This was measured by applying a pressure-sensitive tape (EURO Tape, Century

distributors (P) Ltd.) on the composite coating. Coverage of coated substrate was quantified using Matlab (version 7.1).

2.4.2 Nanoindentation

Young's modulus of composite coating was measured using indenter type Berkovich B3 (Universal Nanomechanical Tester UNAT, ASMEC). Coated sample was measured 15 times at three different forces of 50, 150 and 500 mN each. Young's modulus was inferred from the load–displacement curve for the composite coating.

2.5 Hemolysis assay

The hemocompatibility of coated substrate was evaluated using a method reported in literature [14]. Erythrocytes in normal saline served as a negative control while erythrocytes in distilled water served as a positive control. Percentage Hemolysis was then calculated as

$$\%\text{Hemolysis} = \frac{\text{Absorbance}}{\text{Absorbance}_{100\%\text{Hemolysis}}} \times 100 \quad (1)$$

2.6 Bioactivity studies

The titanium substrates were soaked in simulated body fluid (SBF) prepared as per Kokubo protocol [15] which has similar ionic concentration as in human plasma. The concentration of the ions was (mmol/dm^3) Na^+ 142.0, K^+ 5.0, Mg^{2+} 1.5, Ca^{2+} 2.5, Cl^- 147.8, HCO_3^- 4.2, HPO_4^{2-} 1.0, SO_4^{2-} 0.5. The samples were immersed into SBF for 7, 14 and 21 days. All the samples were incubated at 37°C. Followed by incubation each sample was taken out and examined for the deposition of hydroxyapatite. The coatings were sputter coated with gold alloy. Apatite growth was identified using SEM-EDAX and Micro-raman spectroscopy.

3 Results

3.1 pH optimization

The stability of the suspension is an important factor to achieve good electrophoretic coatings. The pH of ceramic suspension in ethanol was 7.5; there was very little deposition of ceramic particles on cathode, owing to lesser positive charge deposition on ceramic particles. At low pH of 1, although the positive charge deposition was high on ceramic particles, an increased ionic concentration lead to drop-down of applied voltage and hence resulted in lesser ceramic deposition. So, pH optimization was performed using 1 N HCl over a range of pH 1–7.5 at fixed current density of 3 mA/cm^2 and coating duration of 1 min. Quality of the coating was determined by the absence of spalling, pitting and cracks on the coating. From Fig. 1, it was found that at pH of 1.6, the ceramic coating was uniform, dense and without any major surface defects.

3.2 Current density optimization

Current density affects the kinetics of EPD process. Higher current density has the benefit of faster deposition kinetics but at the cost of surface inhomogeneity. Lower current density has slower deposition kinetics but the expected coating is dense, homogeneous and more uniform. Therefore, the ceramic was coated using EPD apparatus at different current densities ranging from 3 to 9 mA/cm^2 and optimized in order to get a uniform coating at a faster rate.

At 7 and 9 mA/cm^2 cracks appeared in the coating in the beginning of the process only. 5 mA/cm^2 produced a uniform coating initially but later on caused spalling. Figure 2 shows that a current density of 3 mA/cm^2 is best suited for producing thick depositions without any deformation.

3.3 Phase analysis and morphological studies

The XRD patterns of AW powder and composite coating are shown in Fig. 3. XRD studies show the presence of different phase as wollastonite (JCPDS 72-2284), HA (JCPDS 09-0432) and TCP (03-0713) in powder and coated sample. Ceramic powder diffraction pattern indicates presence of more crystalline phases with strong diffraction plane (120) of wollastonite and (211) of HA. In the coated sample, Bragg angles of different phases are same as ceramic powder diffraction. Also intensity ratio of powder and coated sample are almost same, so there is no preferred orientation of crystallization during coating. There is an added amorphous band in coated sample which is due to amorphous nature of chitosan. Crystallinity of the apatite–wollastonite powder and composite coating was calculated from XRD pattern and found to be 93 and 65% respectively.

Scanning electron microscopy was employed to investigate the morphological features of the coated sample. It can be inferred from the micrographs (Fig. 4a) that the composite coating has got porous structure and particles are fused together to give irregular morphology. The coating has interconnected pores and thickness of the coat is found to be approximately 10 μm (Fig. 4b). In Fig. 4c, BSE COMPO image of cross section of coating, the darker and lighter patch corresponds to chitosan and AW ceramic particles respectively and there is good homogeneity between the two phases.

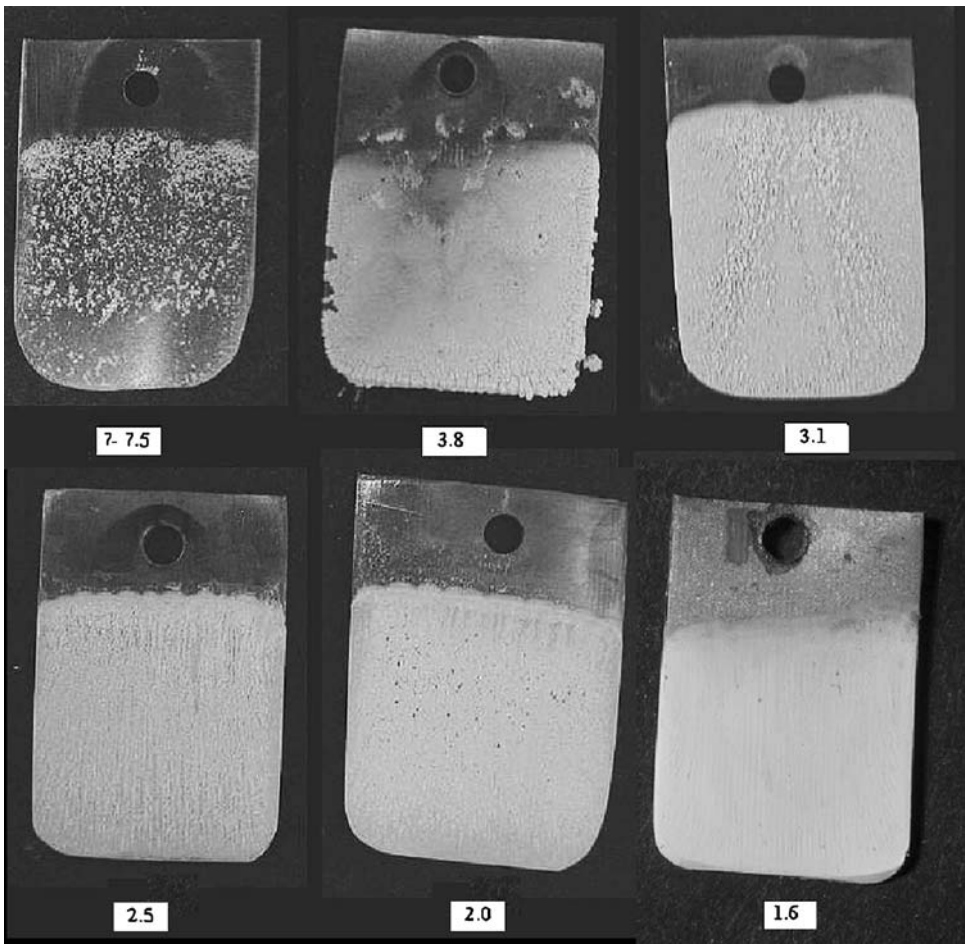

Fig. 1 Photographs of the coatings shown at different pH

3.4 Mechanical strength testing

3.4.1 Tape test

The adhesion of the composite coating on titanium substrate was measured using standard test method (Tape test-D 3359-97). This was done by applying a pressure-sensitive tape (EURO Tape) over cuts made on the coating. In the ceramic coating, the coated area removed was found to be 66% and in the composite coating, the coated area removed was found to be 21%. Classification of adhesion test were evaluated using a scale from 0 to 5 i.e., 0 corresponds to very poor and 5 to very good adhesion respectively. So classification of the coating was done on the basis of standard chart given. With polymer the coating lies in 2B class and without polymer coating it lies in 0B class.

3.4.2 Nanoindentation

Figure 5 displays average load–displacement curves from all measurements for coated sample. The figure shows that the indentation depth increases much faster at smaller loads than at higher loads. Depth-average value of Young's modulus was found to be 9.23 ± 0.94 GPa. Results from still higher depths may be influenced by metallic substrate.

3.5 Hemocompatibility

A biocompatible implant should be hemocompatible also; especially it should not lead to hemolysis, i.e. lysis of the RBCs. The interaction of the coated sample with RBCs was evaluated as these cells serve as model cell membranes. When the values of %Hemolysis were plotted in a bar graph format, the hemocompatibility of the composite coating was found to be approximately 2%.

3.6 Bioactivity

Bioactivity of orthopedic materials is characterized by the capability of forming bone-like apatite in vitro and in vivo. Apatite growth was studied by visualizing different morphological features and elemental composition using SEM-EDAX and confirming phosphate vibrational mode in apatite using Raman spectroscopy. SEM images of composite coating immersed in SBF showed increased apatite

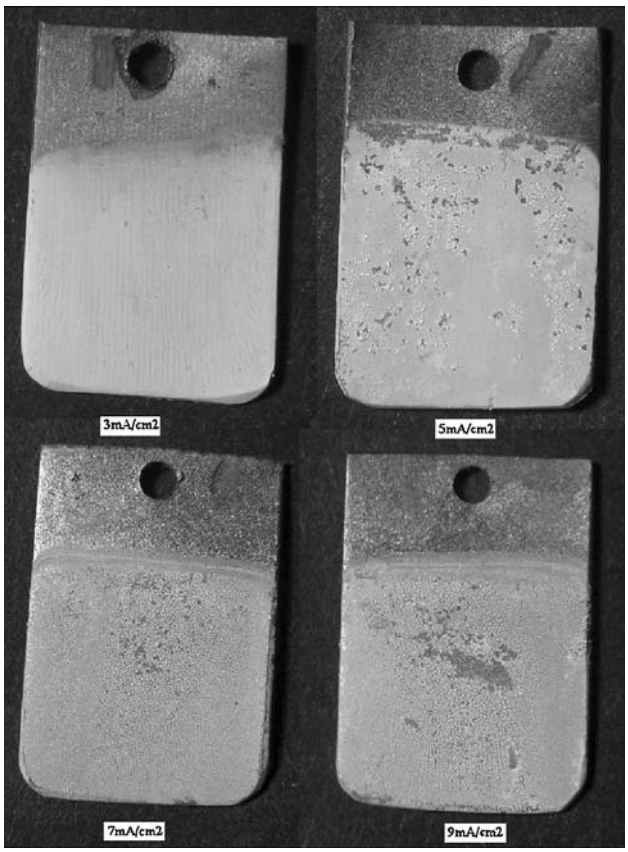

Fig. 2 Photographs of the coatings shown at different current densities

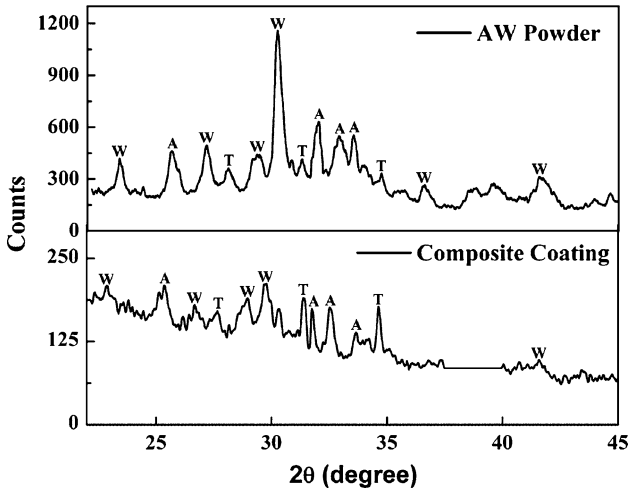

Fig. 3 XRD pattern of apatite–wollastonite powder and composite coating (titanium peaks removed from XRD pattern of composite coating)

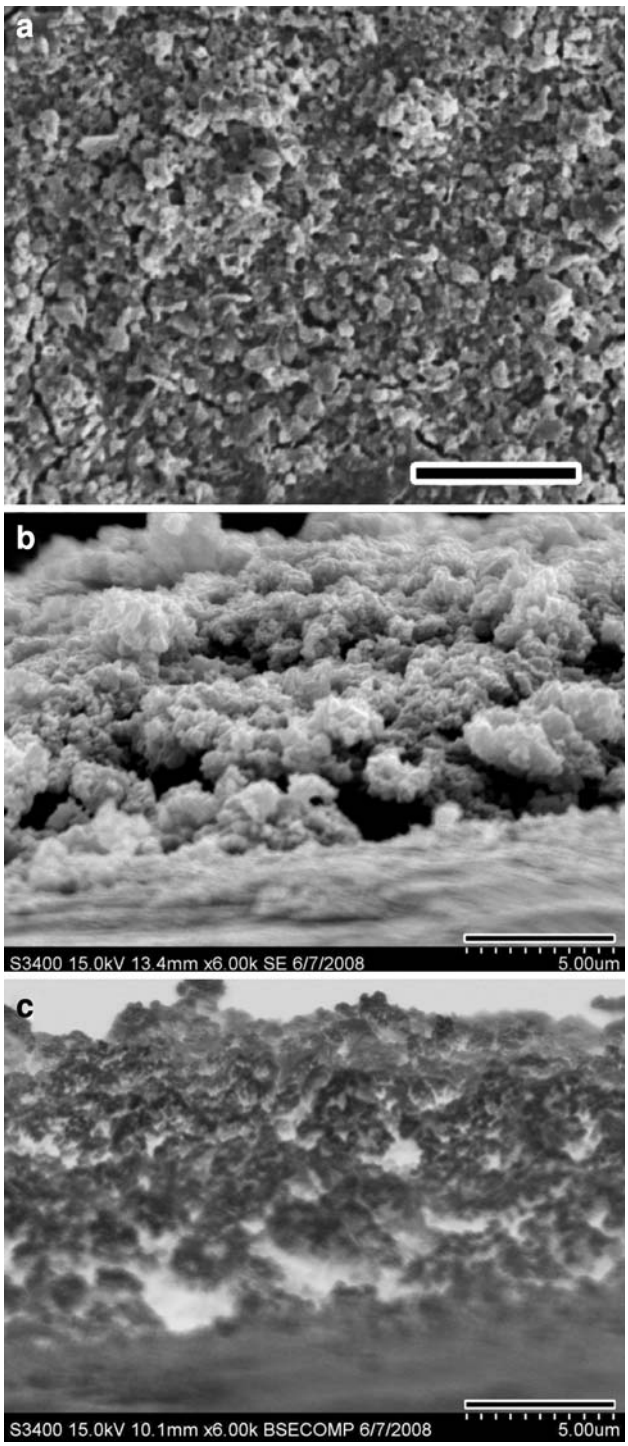

Fig. 4 **a** SEM image of the composite coating (scale bar: 10 μm), **b** SEM image of cross-section of coating (scale bar: 5 μm), **c** BSE COMPO image of cross-section of coating (scale bar: 5 μm)

growth from 7 to 21 days. Ceramic coated and composite coated samples were soaked in SBF for studying their effect on morphology of apatite growth.

From Fig. 6 we see that apatite growth has sheet-like morphology for composite coatings unlike ball-like morphology on AW coated sample which is commonly observed in bioceramics (Fig. 7).

Apatite precipitation was confirmed for all samples from Ca/P ratio of 1.67 measured by EDAX. From EDAX, it was found that Si concentration was large on seventh day

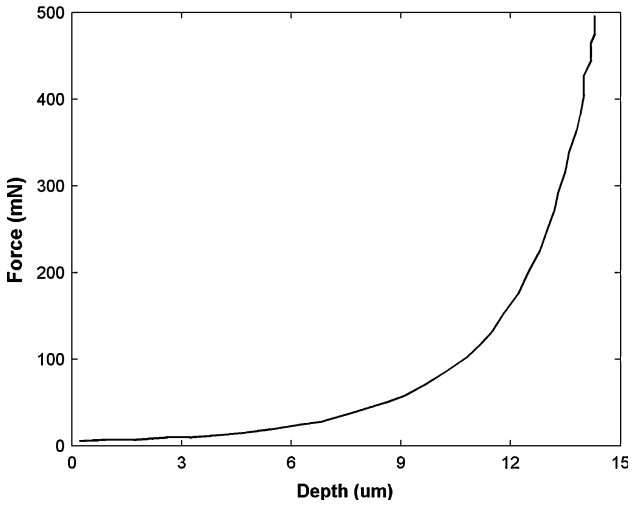

Fig. 5 Load–displacement curve of composite coating

because EDAX was sampling into underlying apatite–wollastonite and hence Si peak is large. However, at 14 and then 21 days SBF samples showed drastic decrease in Si concentration because of thicker apatite layer which reduced the contribution of underlying apatite–wollastonite to the EDAX signal. This gradual decrease in Si content and constant ratio of Ca/P = 1.67 indicated apatite was present and it was growing over the composite coating from 7 to 21 days. Figure 8 explained the mechanism of apatite growth proposed in the composite coating.

Micro-Raman spectroscopy was used to identify different vibrational modes that are Raman active, before and after immersion in SBF for 7, 14 and 21 days.

Figure 9 shows the Raman spectrum of coated samples in the region 250–1100 cm^{-1}. Two intense Raman-scattering bands of hydroxyapatite are identified for control sample, which are associated with two normal modes of frequencies of the PO_4^{-3} tetrahedron viz. symmetric stretching of P–O bonds at 1000 cm^{-1} (v_1 frequency) and asymmetric P–O stretching at 1032 cm^{-1} (v_3 frequency). The small peak towards left of v_1 frequency of PO_4^{-3} belongs to P–O symmetric stretching in $Ca_3(PO_4)_2$ phase in composite coating. For seventh day SBF immersion sample, there is an appearance of broad band at 546 cm^{-1} and a peak at 620 cm^{-1}, which are assigned to breathing vibrations of oxygen atom in Si–O network. The band at 795 cm^{-1} is associated with symmetric stretching vibrational mode of Si–O. Thereafter, for 14 and 21 days there is a progressive decrease in their intensities.

4 Discussion

Electrophoretic process for deposition of ceramic and polymer enables deposition of uniform coatings on substrates of complex shapes. It has been proved as versatile technology for preparing composite coating on metallic substrates with controlled homogeneity and surface roughness [10]. It is an efficient technique for depositing heat sensitive biopolymer. Chitosan has the advantage of providing high flexural strength and also it induces osteoconductive properties [16]. By choosing appropriate proportion of chitosan and AW, bioactive coating with greater mechanical strength can be achieved.

The pH of a suspension affects the particle charge distribution and ionic conductivity of the suspension, which in turn affects electrophoretic mobility of the particles with respect to ions [17]. Thus, dynamics of EPD process can be controlled by selecting appropriate pH of the suspension. Electrophoretic velocity of particle can be related to the charge on the particle and the electric field by a formula

$$v = \frac{EQ}{4\pi r\eta} \tag{2}$$

where, E is applied electric field, Q is particle charge, r is particle radius and η is viscosity of the suspension [18]. For a given concentration of the suspension, its viscosity is invariant and the only thing that varies with the pH of the suspension is the product EQ. At pH 7.5, there is minimum positive charge deposition on particles and finite electric field, i.e., $Q \rightarrow 0$ implies $v \rightarrow 0$, which results in minimum deposition of particles on titanium substrate as is clearly shown in Fig. 1. At pH 1, although the expected positive charge deposition is high the excess of ionic concentration in the suspension will lead to the formation of electric double layer on electrode and will result in an eventual screening down of electric field, i.e., $E \rightarrow 0$ implies $v \rightarrow 0$. Here too, a thin deposition of particles will occur as the electric field is not sufficient for electrophoresis. Hence, there must be an optimum value in between the pH of 1 to 7.5, where the electrophoretic velocity is at a maximum and this has been observed through the uniform dense coat at pH 1.6.

Kinetics of EPD process is governed by applied current density on electrode. Current density influences the rate of mass deposition on cathode and it is followed by Hamaker Equation

$$m = Cvi\rho St \tag{3}$$

where, m is mass deposited, v is electrophoretic mobility, i is current density, ρ is resistivity, S is surface area of electrode and t is time duration of coating [19]. There is a linear relation between rate of mass deposition and current density. At low current density (3 mA/cm^2), the particles get sufficient time to rearrange resulting in a more uniform coating. But as we increase current density to 7–9 mA/cm^2, more particles get deposited with lesser rearrangement resulting in spalling and cracking in the coat.

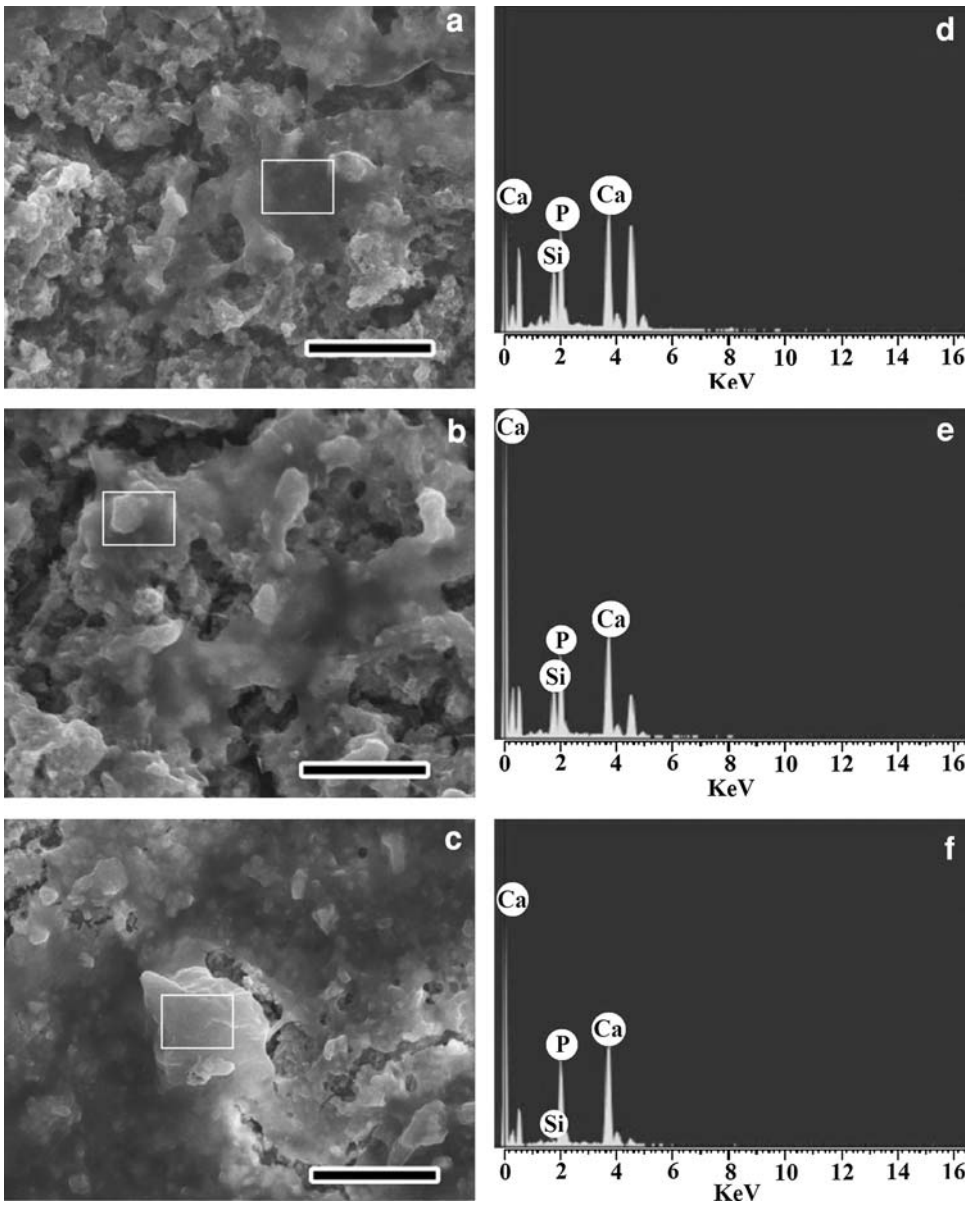

Fig. 6 SEM micrographs of composite coatings immersed in SBF **a** 7th day, **b** 14th day, **c** 21st day (scale bar = 10 μm) and EDAX **d** 7th day, **e** 14th day, **f** 21st day

XRD of ceramic powder confirms the presence of apatite and wollastonite phases. TCP phase is also present in small proportion. XRD pattern of coating shows decreased intensity of peaks and amorphous band; this might be because of very thin coating. Decrease in crystallinity of composite coating observed may be due to incorporation of chitosan. Also there is no preferred orientation of crystallization in any phase of coating because deposition of multi-phase ceramic particle leads to disorder in crystallization planes.

SEM image of composite coating shows interconnected pores. Earlier literature has reported that the interstices and pores in coat are pathways for diffusion of nutrition elements, vascularization and cell growth [20]. The COMPO image shows that AW ceramic is embedded inside chitosan layer providing mechanical strength to composite coating. Hence it can be deduced that EPD is an appropriate processing technique to form an interconnected porous microstructure with desired thickness by controlling the parameters.

Total coating strength is a sum of the adhesive force between coat and substrate and the interparticle cohesive force. To increase the adhesive strength of coating, chitosan was employed as first layer of the composite coating. Polymeric layer increases effective contact area of composite coating as compared to ceramic coating alone. Also within coating layer, ceramic particles are enwrapped in chitosan layer which provide them bulk strength [10]. Chitosan is known to be an effective binder and it provides adhesion of the particles to the substrate and prevents cracking [7].

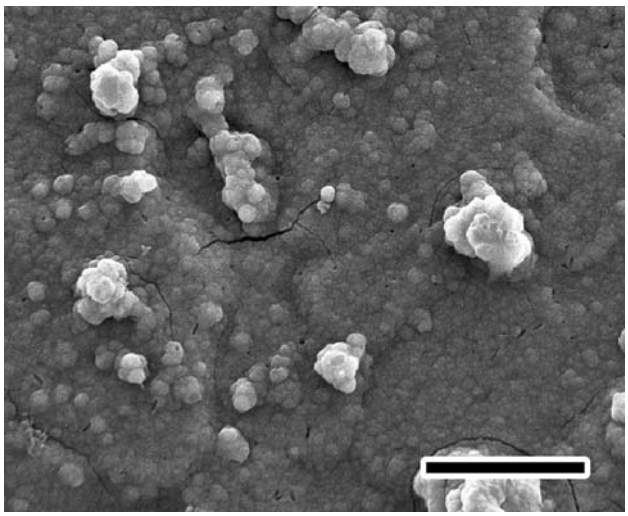

Fig. 7 SEM micrographs of AW coating immersed in SBF for 14 days showing ball-like apatite growth (scale bar = 10 μm)

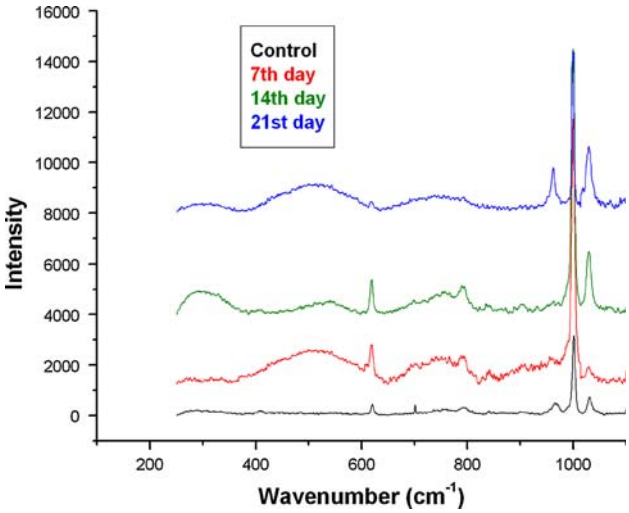

Fig. 9 Raman spectra of control sample and samples immersed in SBF for 7, 14 and 21 days

Young's modulus of the coating is affected by the packing of particles, porosity and composition. Presence of chitosan increases porosity of coat but it also leads to a decrease in Young's modulus due to flexible nature of chitosan as compared to the bulk elastic modulus of AW [21]. It is already reported in literature [21] that Young's modulus decreases due to presence of polymer in AW-polymer composite leading to increase in flexural strength of composite. Thus the incorporation of chitosan causes a decrease in the Young's modulus, but simultaneously increases the adhesive strength of the composite coating.

Hemolysis study is a significant test for biomaterials. The hemolytic reaction level caused by the toxic materials is generally larger than the toxicity reaction level produced in cell culture [22]. The material which causes hemolysis is regarded as a toxic material. According to the standard [23], any material resulting in less than 5% hemolysis is considered hemocompatible. The hemolytic ratio of the composite coating was found to be 2% and thus the coating is hemocompatible.

Investigation on the biological behavior of biomaterials in SBF is considered to be the most efficient method to

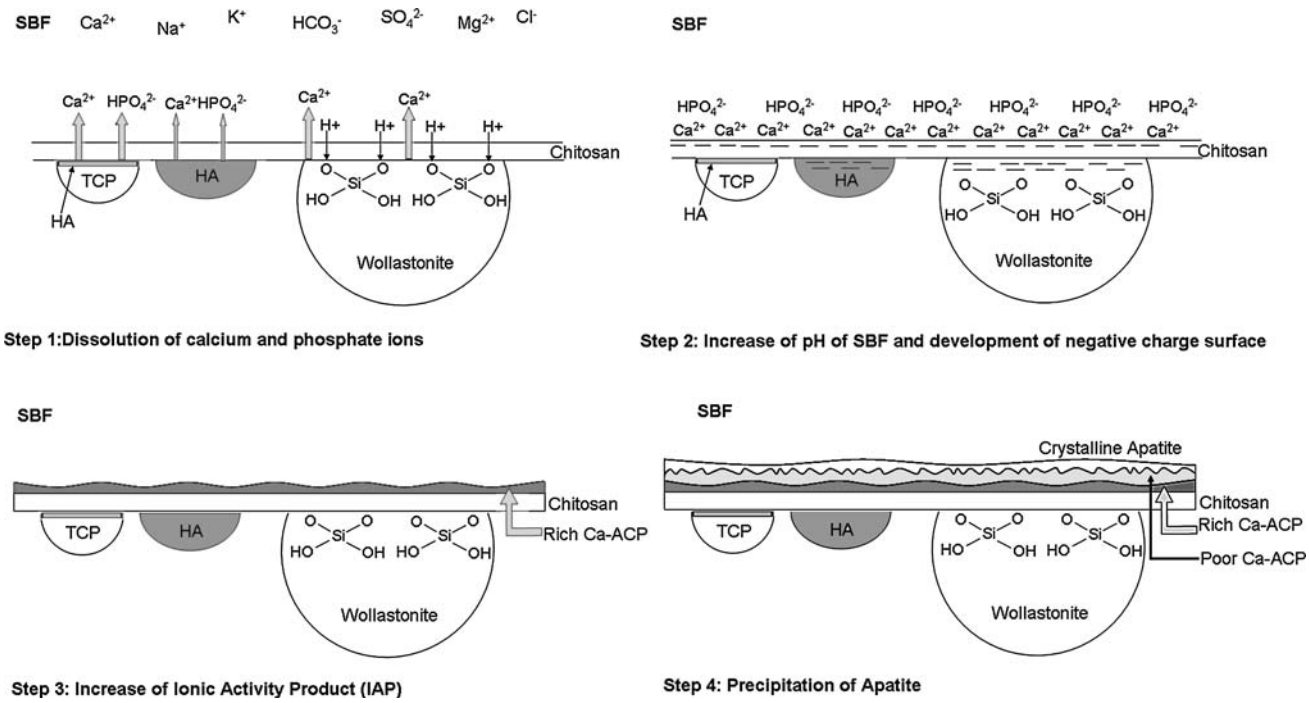

Fig. 8 Schematic of apatite growth mechanism on AW–chitosan composite coating

evaluate their bioactivity in the body environment. Here we are proposing the mechanism of apatite growth on AW-chitosan composite coating and showing the effect of biopolymer on morphology of the apatite. Present composite coating has different phases and each of them have definite role in apatite formation.

4.1 Step 1: dissolution of calcium and phosphate ions

When the coating is immersed in SBF (pH 7.4), ion exchange occurs between the surface layer of the coating and the solution as a result of the different chemical potentials of the ions. The ion exchange in wollastonite phase is coupled with dissolution of calcium ion and absorption of protons leading to formation of silanol group onto its surface [12].

TCP gives insoluble hydroxyapatite and releases calcium and phosphate ions upon hydration during soaking in SBF.

$$4Ca_3(PO_4)_2 + H_2O \rightarrow Ca_{10}(PO_4)_6(OH)_2 + 2Ca^{2+} + 2HPO_4^{2-} \quad (4)$$

As the solubility of hydroxyapatite in water is very low at 37°C, the release of calcium and phosphate ion is less [24].

4.2 Step 2: increase of pH of SBF and development of negative charge surface

Release of calcium and phosphate ions from the ceramic surface and simultaneous consumption of protons from the SBF causes an increase in the pH of the medium. Surface silanol group of wollastonite in high pH medium stabilizes to form $Si–O^-$ group followed with densification of silica layer, which results in an increased surface charge density [12]. As isoelectric point of hydroxyapatite is between pH 7–8.5, at higher pH levels, the phosphate and hydroxyl groups present will have more negative charges on the surface. Similarly, the primary hydroxyl group of chitosan also contributes to the negative charge as it forms $Ch–O^-$ group at pH levels greater than the isoelectric point (pH 6.4) of chitosan (Ch–OH).

$$Ch{-}OH + OH^- \rightarrow Ch{-}O^- + H_2O \quad (5)$$

There is a strong negative charge contribution from polymeric layer which in turn provides dense homogeneous nucleation site for apatite growth.

4.3 Step 3: increase of ionic activity product (IAP)

Increase in ionic concentration of calcium ion, phosphate ion and hydroxyl ion in SBF will increase IAP of apatite and eventually lead to a higher degree of supersaturation in the solution. Negatively charged surface of composite coating will attract calcium ions onto its surface by electrostatic force. These deposited calcium ions will attract their counter ions for apatite formation from SBF.

4.4 Step 4: Precipitation of Apatite

Formation of double layer and increase in IAP of apatite induces rich-calcium phosphate precipitation on coating surface. On successive layers of newly formed Ca–P layer, calcium ion deposition will be lesser as compare to preceding layer. So each successive layer deposited will be of poor-calcium phosphate. As poor-Ca–P has lesser solubility, it is more stable and will eventually convert into crystalline apatite.

Apatite growth was also studied using Raman spectroscopy. The increase in intensity of bands at 546, 620 and 795 cm^{-1} is due to dissolution of calcium ion from wollastonite and formation of silica-rich layer. Thereafter, for 14 and 21 days there is a progressive decrease in their intensities owing to the formation of thick apatite layer onto the composite surface. Broadening of band at 965 cm^{-1}, which corresponds to $Ca_3(PO_4)_2$ phase, for 7 and 14 days is related to the dissolution of calcium phosphate which is the first step in apatite growth mechanism. Again emergence of a peak at a slightly lower frequency on the 21st day is due to the fact that crystallized apatite is supported on rich-calcium phosphate layer.

Thus, the sheet-like morphology of apatite growth is mainly due to densely charge surface of composite coating which may be attributed to the presence of high surface charge density of chitosan. It is generally observed that apatite growth on bioglasses and HA attains a ball-like morphology which is due to presence of grain boundaries. A grain boundary serves as discontinuity for continuous apatite growth. Chitosan might also be masking the grain boundary effect of ceramic particles leading to sheet-like apatite growth.

Further work on in vitro studies on the cellular response of the coating using osteosarcoma cell lines (MG-63) is under progress in our laboratory.

5 Conclusions

A technique for a composite coating of apatite–wollastonite and chitosan on titanium substrates was developed using the ambient temperature and pressure technique of electrophoretic deposition (EPD). The current density and pH of suspension were optimized together to get uniform and crack-free coating. Best results were obtained using a current density of 3 mA/cm^2 and pH of 1.6. The XRD result has confirmed presence of apatite, wollastonite and small amount of TCP phases in both powder and coating,

and furthermore, the coating has reduced crystallinity as compared to AW powder which may be due to addition of chitosan. The coating has porous structure with ceramic particles enwrapped inside the polymer layers. Chitosan incorporation enhanced the adhesive strength of the composite coating. Bioactivity studies showed that apatite growth had sheet-like morphology mainly due to the dense homogenous nucleated sites provided by high surface charge density of chitosan. Sheet-like apatite growth is expected to produce homogenous bioactive surface as compared to ball-like apatite. Chitosan reinforcement in composite coating showed good bioactivity and increased mechanical strength. Considering its economic and simple production, apatite–wollastonite–chitosan composite coating seems to be an attractive candidate to improve the performance of metallic implants.

Acknowledgement This investigation was supported by Research Grant 04DB001 from the Department of Biotechnology, New Delhi 110 003, India.

References

1. Hench LL. Bioceramics: from concept to clinic. J Am Ceram Soc. 1991;74:1487–510.
2. Sena LA, De Andrade MC, Rossi AM, Soares GA. Hydroxyapatite deposition by electrophoresis on titanium sheets with different surface finishing. J Biomed Mater Res. 2002;60:1–7.
3. Liu X, Ding C. Plasma sprayed wollastonite/TiO_2 composite coatings on titanium alloys. Biomaterials. 2002;23:4065–77.
4. Nakamura T, Yamamuro T, Higashi S, Kokubo T, Ito S. A new glass-ceramic for bone replacement: evaluation of its bonding to bone tissue. J Biomed Mater Res. 1985;19:685–8.
5. Yoshii S, Kakutani Y, Yamamuro T, Nakamura T, Kitsugi T, Oka M, et al. Strength of bonding between A-W glass-ceramic and the surface of bone cortex. J Biomed Mater Res. 1988;22:327–38.
6. Peng P, Kumar S, Voelcker NH, Szili E, Smart RC, Griesser HJ. Thin calcium phosphate coatings on titanium by electrochemical deposition in modified simulated body fluid. J Biomed Mater Res. 2005;76A:347–55.
7. Grandfield K, Zhitomirsky I. Electrophoretic deposition of composite hydroxyapatite–silica–chitosan coatings. Mater Charact. 2008;59:61–7.
8. Pang X, Zhitomirsky I. Electrophoretic deposition of composite hydroxyapatite-chitosan coatings. Mater Charact. 2007;58:339–48.
9. Tanabe T, Okitsu N, Tachibana A, Yamauchi K. Preparation and characterization of keratin–chitosan composite film. Biomaterials. 2002;23:817–25.
10. Wang J, De Boer J, De Groot K. Preparation and characterization of electrodeposited calcium phosphate/chitosan coating on Ti6Al4V plates. J Dent Res. 2004;83:296–301.
11. Zhao L, Chang J. Preparation and characterisation of macroporous chitosan/wollastonite composite scaffolds for tissue engineering. J Mater Sci Mater Med. 2004;15:625–9.
12. Liu X, Ding C, Chu PK. Mechanism of apatite formation on wollastonite coatings in simulated body fluids. Biomaterials. 2004;25:1755–61.
13. Pattanayak DK, Prasad RC, Rao BT, Mohan TRR. Apatite Wollastonite–titanium biocomposites: synthesis and in vitro evaluation. J Am Ceram Soc. 2006;89:2172–6.
14. Risbud M, Saheb DN, Jog J, Bhonde R. Preparation, characterization and in vitro biocompatibility evaluation of poly(butylenes terephthalate)/wollastonite composites. Biomaterials. 2001;22:1591–7.
15. Kokubo T, Takadama H. How useful is SBF in predicting in vivo bone bioactivity? Biomaterials. 2006;27:2907–15.
16. Muzzarelli RAA, Zucchini C, Ilari P, Pugnaloni A, Belmonte MM, Biagini G, et al. Osteoconductive properties of methylpyrrolidinone chitosan in animal model. Biomaterials. 1993;14:925–9.
17. Wang C, Ma J, Cheng W, Zhang R. Thick hydroxyapatite coatings by electrophoretic deposition. Mater Lett. 2002;57:99–105.
18. Linder F, Feltz A. Electrophoretic deposition—a method for preparation of semiconducting oxide ceramic layers. Solid States Ionics. 1993;63–65:13–7.
19. Ferrari B, Moreno R, Cuesta JA. A resistivity model for electrophoretic deposition. Key Eng Mater. 2006;314:175–80.
20. Lu JX, Gallur A, Descamps M, Thierry B. Role of interconnections in porous bioceramics on bone recolonization in vitro and in vivo. J Mater Sci Mater Med. 1999;10:111–20.
21. Juhasz JA, Best SM, Brooks R, Kawashita M, Miyata N, Kokubo T, et al. Mechanical properties of glass-ceramic A–W-polyethylene composites: effect of filler content and particle size. Biomaterials. 2004;25:949–55.
22. Yu SR, Zhang XP, He ZM, Liu YH, Liu ZH. Effects of Ce on the short-term biocompatibility of Ti-Fe-Mo-Mn-Nb-Zr alloy for dental materials. J Mater Sci Mater Med. 2004;15:687–91.
23. American National Standard Institute/American Dental Association. ANSI/ADA Specification No. 41. Biological evaluation of dental materials. Washington, DC: ANSI/ADA; 1979.
24. Kim HM, Himeno T, Kokubo T, Nakamura T. Process and kinetics of bonelike apatite formation on sintered hydroxyapatite in a simulated body fluid. Biomaterials. 2005;26:4366–73.